

LYMPHOID NEOPLASIA

Evaluating the impact of *CRBN* mutations on response to immunomodulatory drugs and novel cereblon E3 ligase modulators in myeloma

Yakinthi Chrisochoidou,¹ Andrea Scarpino,¹ Salomon Morales,¹ Shannon Martin,¹ Sarah Bird,^{1,2} Yigen Li,¹ Brian Walker,³ John Caldwell,¹ Yann-Vaï Le Bihan,¹ and Charlotte Pawlyn^{1,2}

¹Division of Cancer Therapeutics, The Institute of Cancer Research, London, United Kingdom; ²Department of Haematology, The Royal Marsden National Health Service Foundation Trust, London, United Kingdom; and ³Division of Hematology and Oncology, Melvin and Bren Simon Comprehensive Cancer Center, Indiana University School of Medicine, Indianapolis, IN

KEY POINTS

- *CRBN* missense mutations identified in patients were modeled to explore their effect on *CRBN* function with IMiD and CELMoD therapy.
- Mutations led to complete loss of *CRBN* function, no apparent effect on *CRBN* function, or IMiD resistance but with retained CELMoD activity.

Immunomodulatory drug (IMiD) resistance is a key clinical challenge in myeloma treatment. Previous data suggest almost one-third of myeloma patients acquire genetic alteration of the key IMiD effector cereblon (*CRBN*) by the time they are pomalidomide refractory. Some events, including stop codons/frameshift mutations and copy loss, have clearly explicable effects on *CRBN* protein function. Missense mutations have also been reported throughout the length of *CRBN* but their functional impact has not been systematically studied. This study modeled selected missense mutations and examined their effect on *CRBN* function also analyzing whether any mutations deleterious to IMiD action could be overcome using the novel cereblon E3 ligase modulators (CELMoDs). Three patterns of response to missense mutations were apparent: mutations that led to complete loss of *CRBN* function for all agents, those that had no effect on *CRBN* function, and those with agent-dependent effect on *CRBN* function. The latter group of 4 mutations were profiled in more detail with confirmatory experiments demonstrating an ability of the more potent CELMoDs to lead to neosubstrate degradation and cell death even though IMiDs were not active. Dynamic modeling based on a newly generated crystal structure of the DDB1/*CRBN*/lenalidomide complex, with greater resolution than those

published to date, helped to understand the impact of these mutations. These results have important implications for the interpretation of *CRBN* sequencing results from patients for future therapy decisions, particularly differentiating those who may, despite relapsing on IMiDs with *CRBN* mutations, have the potential to still benefit from the use of CELMoD agents.

Introduction

Immunomodulatory drugs (IMiDs) have revolutionized the treatment of multiple myeloma and are the backbone of most current standard and experimental combination therapies at all stages of the disease including as maintenance therapy strategies.¹ The term IMiDs refers to thalidomide, the first IMiD to be used for myeloma treatment, and its analogs lenalidomide (Len) and pomalidomide (Pom). Next-generation analogs, termed cereblon E3 ligase modulators (CELMoDs), iberdomide (Iber, CC-220^{2,3}), and mezigdomide (Mezi, CC-92480),^{4,5} are currently being assessed in phase 3 clinical trials. IMiDs and CELMoDs function as molecular glues using the CRL4^{CRBN} E3 ligase, a complex formed of proteins Cullin-4A (CUL4A), RING box protein 1 (ROC1/RBX1), DNA damage-binding protein 1

(DDB1), and cereblon (CRBN). CRBN mediates protein degradation by acting as the substrate receptor for this complex, leading to the ubiquitination of substrates and their subsequent proteasomal degradation⁶⁻⁸ (Figure 1A).

CRBN is a 51kDa protein with 3 domains: a N-terminal Lon protease-like domain, a central helix-bundle subdomain that allows binding of CRBN to DDB1, and a C-terminal thalidomide-binding domain (TBD). The TBD harbors a β -tent fold stabilized by a zinc atom and contains a hydrophobic tri-tryptophan (3-Trp) pocket formed at amino acids 380, 386, and 400.¹³⁻¹⁵ This pocket has been described as the binding site of C-terminal cyclic imide post-translational modifications in the natural substrates of CRBN, constituting the natural degron that triggers protein ubiquitination by the CRL4^{CRBN} complex.

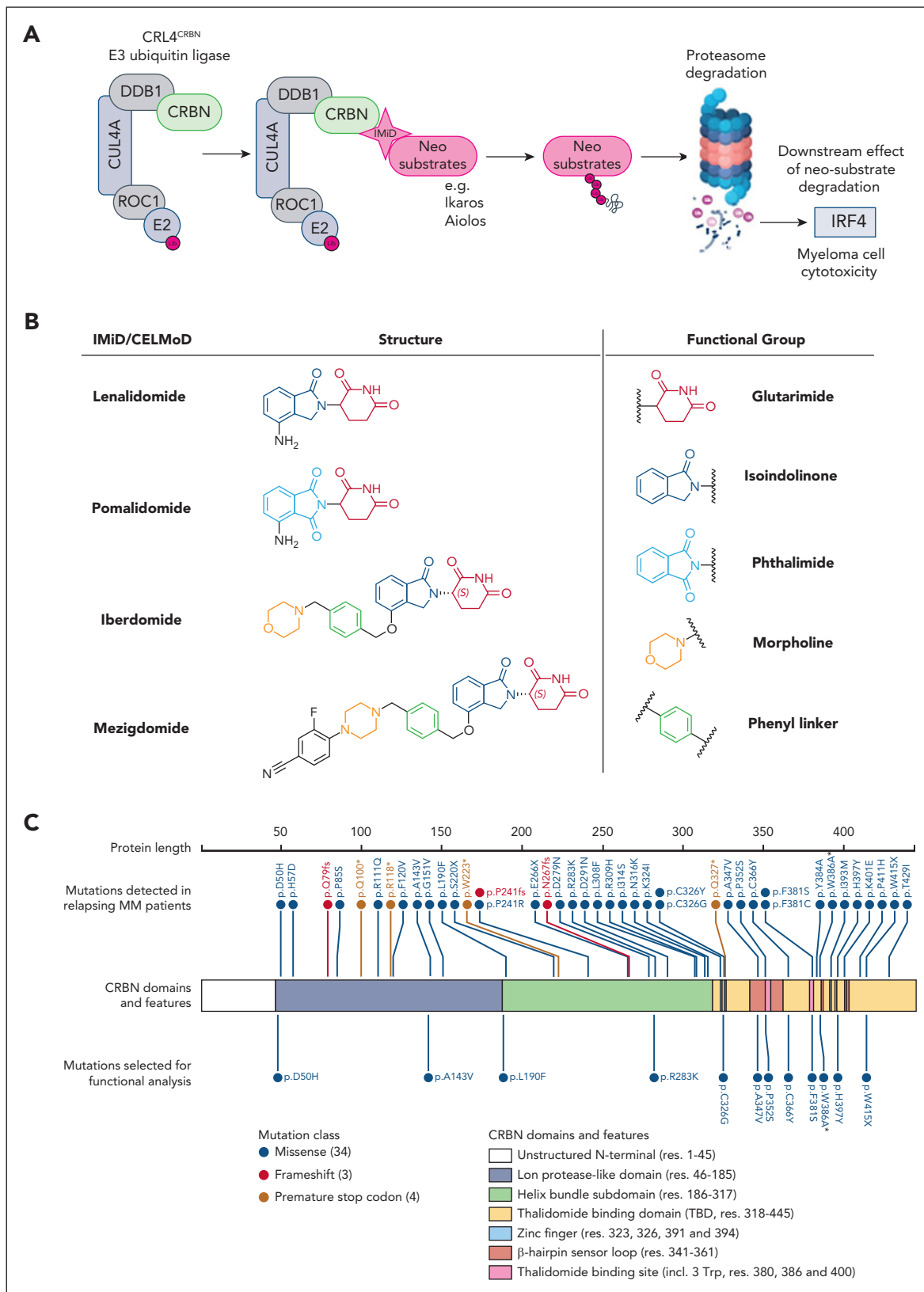


Figure 1. Overview of IMiD mechanism of action, the investigated compounds and reported CRBN mutations. (A) Schematic of the CRL4^{CRBN} E3 ubiquitin ligase complex and the IMiD mechanism of action that results in myeloma cell cytotoxicity. Figure created with BioRender.com. (B) Chemical structures for Len, Pom, iberdomide (CC-220), and Mezi (CC-92480). Len and Pom share a common glutarimide ring and differ only through the replacement of the isoindolinone in Len by a phthalimide in Pom.⁹ This difference leads to altered neosubstrate degradation, with Len being the only one able to potentially degrade the kinase CK1 α in cells.¹⁰ The chemical composition of the next-generation CELMoDs has led to higher CRBN-binding affinity. Iber achieves that through its additional phenyl and morpholino moieties, which extend the interactions with the β -hairpin sensor loop resulting in enhanced stabilization of the closed conformation of CRBN and ultimately increased neosubstrate ubiquitination and

The glutarimide ring present in IMiDs mimics this natural degron, allowing for the binding of IMiDs to CRBN.¹⁶ Once an IMiD is bound in the 3-Trp pocket of CRBN, this induces the structuration of a β -hairpin sensor loop (residues 341-361), which stacks against the drug and induces a structural rearrangement of CRBN into a closed conformation where the N-terminal Lon protease-like domain and the C-terminal TBD come in close proximity.¹¹ This structural rearrangement leads to the creation of a neomorphic surface on CRBN that alters its substrate specificity, triggering the recruitment of neosubstrates to CRBN leading to their ubiquitination and degradation. All IMiD and CELMoD-induced CRBN neosubstrates known to date contain a structurally similar β -hairpin degron, which interacts with the phthalimide or isoindolinone moiety of the compounds through a conserved glycine.^{10-12,17-19} Most of the known neosubstrates of CRBN are transcription factors where the degron is embedded within a C2H2 zinc finger. In myeloma this includes the B-cell transcription factors Ikaros (IKZF1) and Aiolos (IKZF3)¹² whose degradation leads to the down-regulation of interferon regulatory factor 4 (IRF4) and myc proto-oncogene protein (c-MYC), which are critical for myeloma cell survival.^{6,7,11,20}

Key structural differences between IMiDs and CELMoDs (Figure 1B) result in differences in potency and the range of neosubstrates that can be degraded. The need for compounds with increased CRBN-binding affinity was driven by treatment-refractory patients. Low CRBN expression has been observed in the IMiD refractory state,²¹ and more potent compounds could be hypothesized to be able to overcome this by binding lower levels of CRBN more efficiently to achieve an effect. However, almost one-third of patients with myeloma acquire CRBN mutations by the time they become Len and Pom refractory.^{22,23} Some events, including the induction of stop codons, frameshift mutations, and copy loss, have clearly explicable effects on CRBN function, but many missense mutations were also reported at variable cancer clonal fractions for which the effects on CRBN function remain unknown.²³

This study aimed to understand which missense mutations are deleterious to CRBN function and whether any mutations deleterious to IMiD action could be overcome with CELMoDs using structural analysis, molecular modeling, and functional validation.

Materials and methods

Functional assessment

Cell culture methods and generation of cell lines are described in the supplemental Methods, available on the *Blood* website. For all GI₅₀ (growth inhibitory) assays, cells were seeded at 10⁵ cells per well and treated with 1:4 serial dilutions of IMiD/CELMoD used in their optimal concentration range based on the GI₅₀ in parental MM1.s: Len at a maximum concentration of

20 μ M, Pom at a maximum concentration of 8 μ M, Iber (CC-220) at a maximum concentration of 2 μ M, and Mezi (CC-92480) at a maximum concentration of 1 μ M. Len and Pom were purchased from Fluorochem Ltd. Iber and Mezi were synthesized in-house using literature procedures. Cell viability measurements were obtained after 5-day incubation with IMiD/CELMoD using the CellTiter-Blue cell viability assay (Promega). To assess CRBN mechanism of action, 10⁶ cells were treated for 24 hours with 10 μ M Len, 1 μ M Pom, 0.1 μ M Iber, 0.01 μ M Mezi, or dimethyl sulfoxide (Sigma-Aldrich) before harvesting for either quantitative reverse transcription polymerase chain reaction (Hs01056533_m1 TaqMan IRF4 gene expression probe) or immunoblotting analysis (supplemental Table 1).

From the IMiD-sensitive MM1.s cell line, 2 CRBN knock out (KO) models were generated using CRISPR-Cas9 (MM1.s^{CRBNKO} clone 1 and MM1.s^{CRBNKO} clone 2). Successful KO of CRBN was confirmed using targeted next-generation sequencing (supplemental Figure 1A).²⁴ Functional validation of KO was confirmed given that there was no viability response (supplemental Figure 1B) or neosubstrate degradation with IMiD/CELMoDs (supplemental Figure 1C-D). Absence of CRBN protein expression was confirmed (supplemental Figure 1C-D) and there was no difference in the doubling times of the KO clone cell lines compared with control (supplemental Figure 1E). An additional CRBN^{KO} model was generated for validation using the KMS11 cell line. The KMS11 cell line is intrinsically IMiD resistant but its CRBN is fully functional with degradation of the neosubstrates Ikaros and Aiolos maintained, meaning this model could be used to validate protein-level changes but not viability changes. In KMS11^{CRBNKO} absence of CRBN protein expression was confirmed along with loss of Ikaros and Aiolos degradation compared with parental cells. All 3 KO models were then transduced with the mutant/wild-type (WT) plasmids to generate stable re-expression of CRBN to similar levels (supplemental Figure 2).

Structural analysis and molecular modeling

Publicly available crystallographic structures of CRBN/DDB1 complex bound to Len and CK1 α (Protein Data Bank [PDB] code 5FQD),¹⁰ bound to CC-885 and GSPT1 (PDB code 5HXB),¹⁷ and bound to Pom and IKZF1 or ZNF692 (PDB code 6H0F and 6H0G,¹² respectively) were overlaid on CRBN TBD using Pymol.²⁵ All mutations previously identified in patient data sets^{23,26-29} were mapped on this overlay to consider their likely effect, based on the types of mutation, their position on CRBN, and proximity vs the molecular glues and neosubstrates.

Given that the accuracy of molecular modeling can be significantly affected by the quality of the starting protein 3D model and most of the publicly available compound-bound structures of the human CRBN/DDB1 complex are of moderate resolution (mostly >3 Å), a novel X-ray crystal structure of this complex (with Len bound) at the improved resolution of 2.00 Å was

Figure 1 (continued) degradation.^{2,11} The design of Mezi further improves this by creating additional interactions with CRBN, which results in a further improvement in the degradation efficiency and kinetics.^{4,11} (C) Linear depiction of the CRBN protein; above are noted all CRBN mutations (n = 34) that have been reported in patients and below CRBNs are the 12 mutations investigated in this study. The color of the mark denotes the type of each mutation. Regarding mutation p.W415X, Gooding et al²³ reported this mutation as W415X. Among the potential reported mutations for this region, it was selected to mutate Trp (W) into a Gly (G) as the most potentially harmful to proper folding and stability of CRBN due to the size difference of these residues. Figure generated using the ProteinPaint <https://proteinpaint.stjude.org/> software by St. Jude Children's Research Hospital. *Mutation not encountered in patients but added as an experimental positive control. One of the 3 Trp forming the IMiDs binding pocket, its mutation to an alanine has been previously demonstrated to functionally inactivate CRBN.^{7,13}

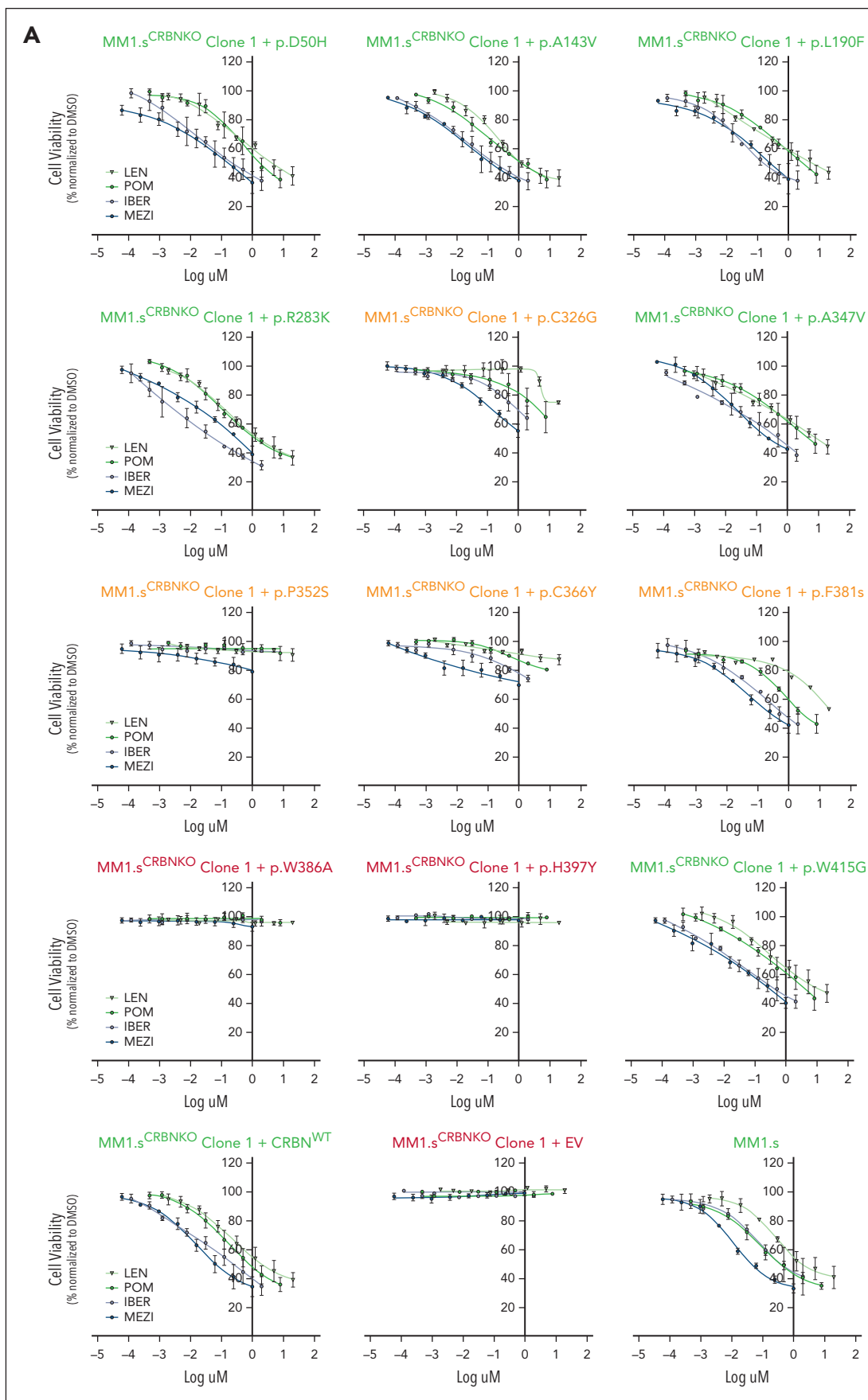


Figure 2. The impact of CRBN mutations on the cell viability of IMiD-sensitive myeloma cell lines. (A) Growth inhibitory (GI50) cell viability measurements for the MM1.s^{CRBNKO} clone 1 cell lines each one expressing a differently mutated CRBN, CRBN^{WT}, or empty vector (EV) in comparison with parental MM1.s. The color of the title for each graph denotes the effect of each mutation on cell viability, where green is associated with reduction in cell viability comparable with parental MM1.s, red denotes no

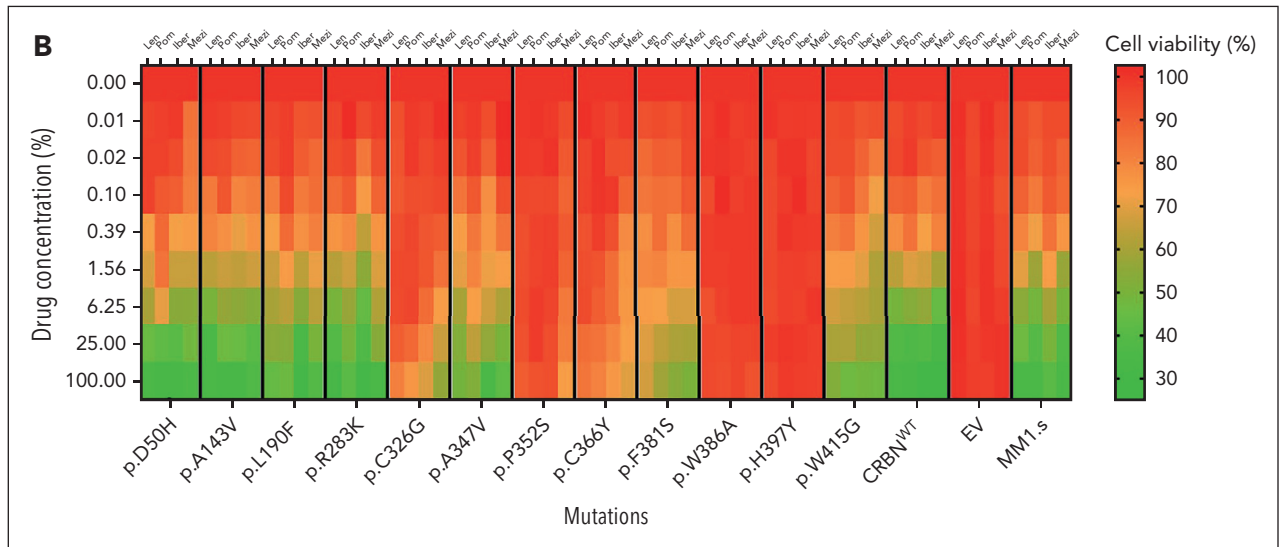


Figure 2 (continued) reduction in cell viability, and orange highlights the mutations whose presence leads to partial reduction in cell viability. Cells were treated with dimethyl sulfoxide (DMSO) or increasing concentrations of Len (maximum concentration 20 μ M), Pom (maximum concentration 8 μ M), Ibr (maximum concentration 2 μ M), and Mezi (maximum concentration 1 μ M) for 5 days. Cell viability was determined using the CellTiter-Blue assay and expressed as a % of DMSO control. Results are the mean \pm standard error of the mean (SEM) of $n = 4$ biological replicates. (B) Heat map summarizing the results shown in Figure 2A but with the drug concentration expressed as a percentage of the maximum for that cell line, Len 100% = 20 μ M, Pom 100% = 8 μ M, etc, and cell viability expressed as a percentage of DMSO control.

generated and deemed to be of sufficient quality to enable molecular modeling. The details of the protein production, purification, crystallization, crystallographic data collection, and structure determination can be found in the supplemental Methods.

Protein structures were prepared with the Protein Preparation Workflow³⁰ in Maestro (Schrödinger Suite v2023-3³¹). Residue mutations were applied to the prepared reference structure using the 3D Builder in Maestro. Molecular dynamics (MD) simulations were conducted using the Desmond³² package after preparation with the System Builder. Each complex was neutralized, immersed in a TIP3P water box of orthorhombic shape extending to 10 Å in each direction and prepared under periodic boundary conditions with the OPLS4 force-field. The solvated systems were subjected to a default relaxation protocol before 100 nanoseconds MD simulation runs performed in 5 independent replicas with randomized velocities in the NPT ensemble at 1.01325 bar and 300 K. Representative conformations were obtained by clustering MD trajectory frames (1000 frames/MD) on binding site residues heavy atoms using the `trj_cluster.py` script. Root-mean-square deviation (RMSD) and clash volume calculations were performed on MD trajectory frames using the analysis and interactions modules in the Schrödinger Python Application Programming Interface (API). The IKZF1 degron used for clash volume analysis was defined as the G-5 to G+1 residue sequence (QCNQCGA) from PDB 6h0f chain C. Molecular visualizations were produced with Molecular Operating Environment (MOE).³³

Results

Selection of mutations for functional analysis

A list of 34 CRBN mutations identified in patients relapsing after IMiD treatment was compiled from previous studies^{23,26-29}

(Figure 1C; supplemental Table 2). Of the 28 missense mutations, a subset of 12 mutations were selected (11 patient-derived + p.W386A-positive control) that occurred across the full length of the protein (Figure 1C; supplemental Table 3). Three of these residues directly participate in the binding of the IMiDs (P352) or are in close proximity and participate in the stabilization of the IMiDs' 3-Trp binding pocket (F381 and H397). A second set of 3 mutations included residues potentially important for the stability and/or proper folding of CRBN without being in close proximity to the IMiDs' or neosubstrates' binding sites. This includes C326, whose mutation would disrupt the Zn finger at the core of the TBD fold, 2 other residues A347 (relatively buried) and C336 (solvent exposed) that are both part of the β -hairpin sensor loop, and W415 (relatively buried), which is also potentially important for the stability and folding of CRBN. Despite being far away from the IMiDs and neosubstrates interaction areas, residue L190 was selected given that it is located at the interface between CRBN and DDB1, so mutation could have an impact on the integrity of the CRL4^{CRBN} E3-ligase complex. Three additionally selected residues are surface exposed and far away from the IMiDs and neosubstrate-binding sites (D50, A143, and R283).

Determining the effect of CRBN mutations on function

The expression of WT CRBN resensitized MM1.s^{CRBNKO} cells to IMiDs/CELMoDs with degradation of Ikaros, Aiolos, and ZFP91; downregulation of MYC and IRF4; and a similar effect on cell viability to that seen in parental MM1.s (supplemental Figure 3A-C). In contrast, the mutation selected as a positive control, p.W386A,¹³ seemed to completely inactivate CRBN with no change in Ikaros/Aiolos/ZFP91/MYC protein levels nor IRF4 messenger RNA level and no effect on cell viability after incubation with all IMiDs/CELMoDs (supplemental Figure 3D-E).

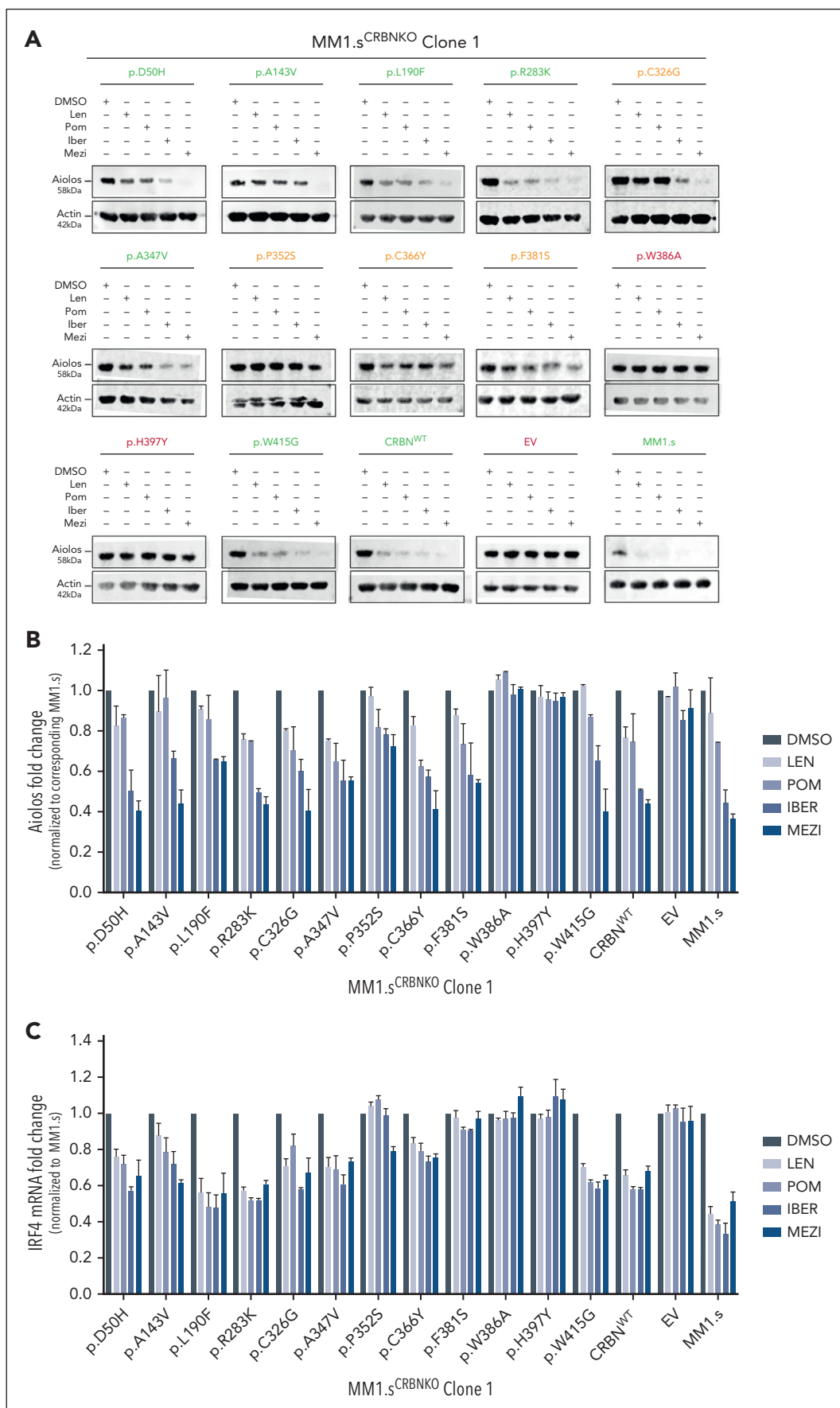


Figure 3.

For the remaining investigated mutations, 3 patterns of response were observed based on viability response and CRBN functional validation^{7,13,34}: (1) mutations that results in complete loss of CRBN function, (2) mutations with no effect on CRBN function, and (3) mutations that seemed to have an intermediate effect (Figures 2 and 3). These are discussed in the context of their spatial localization on CRBN (supplemental Figures 4 and 5). The patterns of neosubstrate protein degradation associated with each CRBN mutation were additionally validated in an independent cell line model, KMS11^{CRBNKO}.

Mutations leading to loss of CRBN function Complete loss of CRBN function was seen with p.H397Y, which had the same effect as the positive control p.W386A, preventing all IMiD and CELMoD activity. In the p.H397Y cell lines, all IMiDs and CELMoDs led to no reduction in cell viability (Figure 2; supplemental Figure 6; mutations highlighted in red), no Aiolos degradation (Figure 3A-B; supplemental Figures 7A-B and 9), and no subsequent IRF4 downregulation (Figure 3C; supplemental Figure 7C). The analysis of available CRBN structures shows that H397 is a scaffolding residue that interacts with and stabilizes W400, a component of the 3-Trp binding pocket, stabilizing its side chain in a conformation that enables the binding of IMiDs (supplemental Figure 4B). The conversion of histidine into the bulkier tyrosine residue would generate a clash with W400, altering the side chain orientation (rotamer), which would likely induce the collapse of the 3-Trp pocket. The other favorable possible rotamers of a tyrosine would remove the scaffolding function of H397 in maintaining W400 in the right conformation for IMiD binding and would occupy the neosubstrates degon binding site, in either case effectively disrupting the activity of CRBN (supplemental Table 3).

Mutations with no apparent effect on CRBN function Some CRBN mutations seemed to have no deleterious effect on CRBN function with a reduction in cell viability seen with all IMiDs and CELMoDs similar to that observed with WT CRBN (Figure 2; supplemental Figure 6; mutations highlighted in green). For most of these residues, CRBN functionality was also observed in the degradation of Aiolos (Figure 3A-B; supplemental Figures 7A-B and 9) and subsequent IRF4 downregulation (Figure 3C; supplemental Figure 7C). The cell lines expressing these mutations regained CRBN function similar to that seen with WT CRBN re-expression. Of note, Aiolos degradation for p.A143V seems slightly reduced but not enough to affect the viability response. These mutations included all those located in the Lon protease-like domain and helix-bundle subdomain p.D50H, p.A143V, p.L190F, and p.R283K. Structural analysis could rationalize the effect of some of these mutations given that amino acids D50, A143, and R283 are not only distal to both IMiD and neosubstrate-binding sites, but as surface residues their mutation was likely to be spatially

accommodated (supplemental Figure 5A-B,D; supplemental Table 3). Mutation p.L190F was also found to be tolerated, whereas structural analysis indicated that the bulkier phenylalanine instead of leucine could potentially perturb the interaction between CRBN and DDB1, and hence could have destabilized the CRL4^{CRBN} E3 ligase complex (supplemental Figure 5C). However, we found no evidence of this in the functional assays (supplemental Table 3). Similarly, p.A347V and p.W415G did not alter CRBN function despite being located in the TBD (supplemental Figure 5E-F). Although both amino acid positions are far away from the IMiDs and neosubstrate-binding areas, the residues are relatively buried so could have been expected to have an impact on the folding and/or stability of CRBN (supplemental Table 3).

Mutations with an agent-dependent effect on CRBN function The remaining 4 mutations studied, p.C326G, p.P352S, p.C366Y, and p.F381S, seemed to only partially abolish CRBN activity (Figures 2 and 3; supplemental Figures 6 and 7; mutations highlighted in orange). Therefore, additional profiling was conducted in these cell lines, including examining the degradation of additional neosubstrates Ikaros and ZFP91, the downregulation of MYC (Figure 4A; supplemental Figure 8A), and the cell proliferation responses summarized compared with WT and positive control p.W386A (Figure 4B; supplemental Figure 8B). Significant lowering of CRBN activity was observed with IMiDs Len and Pom, yet some response was retained particularly with CELMoDs, in terms of neosubstrate degradation (Figures 3A-B and 4A; supplemental Figures 7A-B, 8A, and 9), IRF4 downregulation, and reduction in cell viability (Figure 4B; supplemental Figure 8B).

Although CRBN function was severely reduced with IMiDs, both CELMoDs were able to rescue the function of CRBN with p.C326Y and p.F381S. The former cysteine is part of a Zn finger motif, which is core to the β -tent fold of the TBD and thought to be crucial in maintaining the functional integrity of CRBN (Figure 4C; supplemental Table 3). Similarly for p.F381S (Figure 4F), the conversion of phenylalanine, a hydrophobic aromatic residue playing a scaffolding role at the heart of the TBD and in immediate proximity to the 3-Trp pocket, to serine, a hydrophilic residue of smaller size, was predicted to compromise the integrity of CRBN, which is indeed what was observed with IMiDs, yet both CELMoDs could retain their degradation and reduction in cell proliferation activity albeit not to the same magnitude as with CRBN^{WT} re-expression (Figure 4B; supplemental Table 3).

For the mutation p.P352S, the switch of proline to the polar amino acid serine was found to critically interfere with the activity of Len, Pom, and Iber. This is in line with the structural analysis, given that P352 is in direct interaction with the isoindolinone or phthalimide cores of the IMiDs and CELMoDs,

Figure 3. The impact of CRBN mutations on neosubstrate degradation after IMiD/CELMoD treatment. Approximately 1×10^6 cells from each MM1.s^{CRBNKO} clone 1 cell line (expressing a differently mutated CRBN, CRBN^{WT}, or EV) and the parental MM1.s cell line were drug treated (10 μ M Len, 1 μ M Pom, 0.1 μ M Iber, 0.01 μ M Mezi, or DMSO) for 24 hours before harvesting for either western blotting or RNA extraction. (A) Immunoblotting results for the neosubstrate protein Aiolos in the investigated cell lines after IMiD/CELMoD treatment. For each cell line, protein-level measurements for all treatments are calculated as fold change normalized to the corresponding DMSO-treated control. The color of the title for each blot denotes the effect of corresponding mutation on protein levels, where green is associated with expression comparable with parental MM1.s (shown in lower right corner), red denotes no reduction in protein levels, and orange highlights the mutations whose presence leads to partial reduction in protein levels. Blots shown are representative of 3 biological replicates. (B) Optical densitometry quantification of the immunoblotting results shown in Figure 3A for the 3 biological replicates. Data are shown as mean \pm SEM. (C) Quantitative reverse transcription polymerase chain reaction results for the messenger RNA expression levels of transcription factor IRF4 after IMiD/CELMoD treatment. Data are shown as mean \pm SEM of $n = 3$ biological repeats.

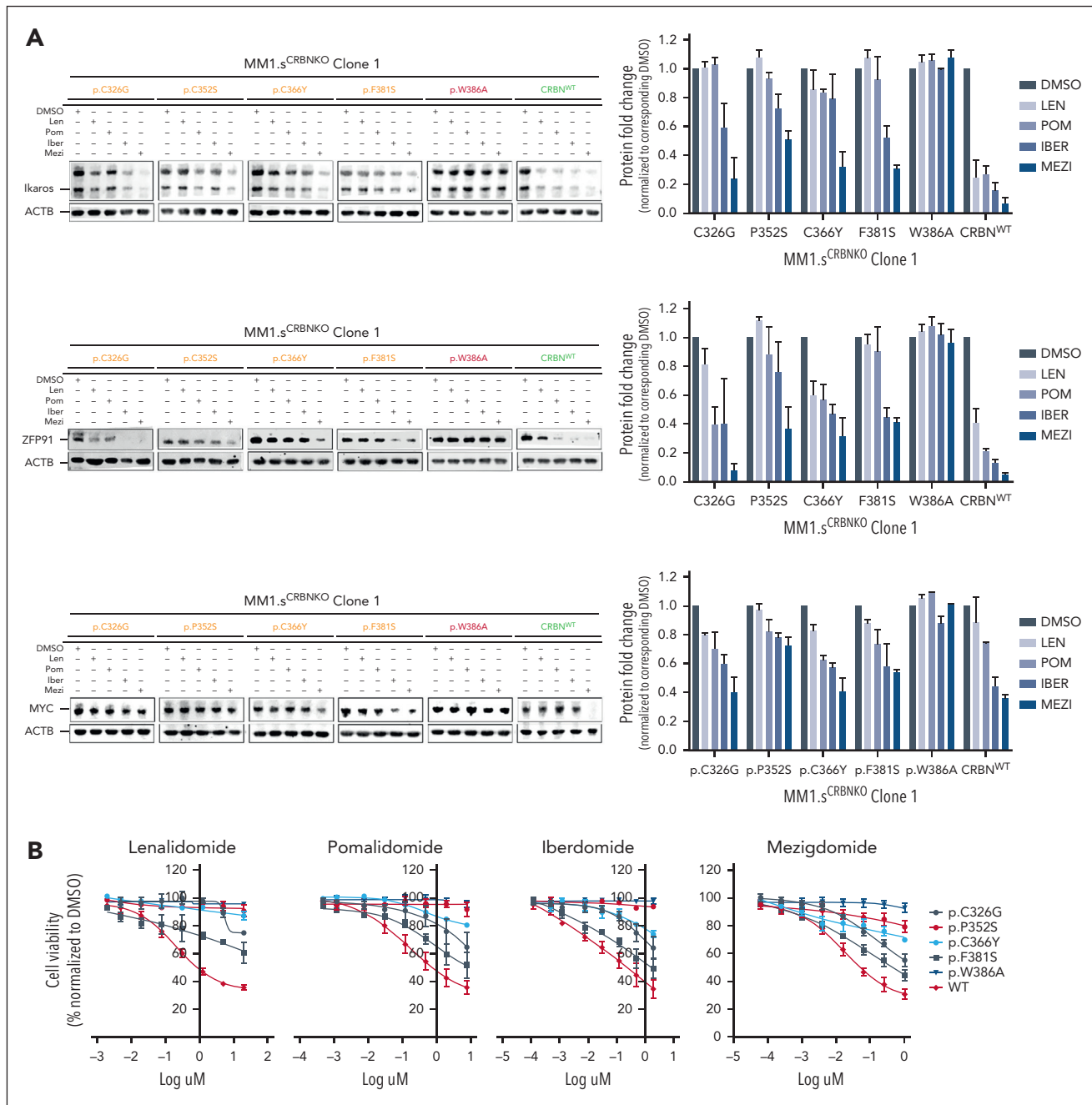


Figure 4. Compilation of the in vitro results and structural analysis of the CRBN mutations that demonstrated partial impact on CRBN function. (A) Immunoblotting results for CRBN neosubstrates Ikaros and ZFP91 and for transcription factor MYC for all CRBN mutations that demonstrated partial CRBN function. The blots for p.W386A and CRB^{WT} have been included as negative and positive control, respectively. Cells were drug treated (10 μ M Len, 1 μ M Pom, 0.1 μ M Iber, 0.01 μ M Mezi, or DMSO) and harvested 24 hours after IMiD/CELMoD treatment for sodium dodecyl sulfate-polyacrylamide gel electrophoresis (SDS-PAGE)/western blotting. Left panel: data shown are representative of 3 biological repeats. Right panel: optical densitometry quantification of the 3 biological replicates. (B) GI50 cell viability results, displayed per compound, for all cell lines whose CRBN mutation demonstrated partial CRBN function in comparison with p.W386A (negative control) and CRB^{WT} (positive control). All cell lines were treated with DMSO or increasing concentrations of Len (maximum concentration at 20 μ M), Pom (maximum concentration 8 μ M), Iber (maximum concentration 2 μ M), and Mezi (maximum concentration 1 μ M) for 5 days. Cell viability was determined using the CellTiter-Blue assay. Results are the average \pm SEM of n = 3 biological replicates. (C-F) Spatial localization of the CRBN mutations that demonstrated an intermediate/variable effect on CRBN function with respect to the IMiDs and neosubstrate-binding sites. The presented figure is a composite figure generated by overlaying our high-resolution crystallographic CRBN/DDB1 structure bound to Len (where CRBN is present in its closed conformation, PDB code 9JFX), with the publicly available crystallographic structure of neosubstrate Ikaros bound to CRBN/DDB1/Pom complex (where CRBN is present in its open conformation, PDB code 6H0F¹²). CRBN is represented in gold, Ikaros in orange, DDB1 in gray, Len in cyan, the 3 Trp defining the IMiD's binding pocket in light blue, Zn²⁺ atoms as gray spheres, and the position of the mutations in magenta. Figures were generated with Pymol.²⁵ (C) Localization of CRBN Cys326, mutated to Gly in patients. (D) Localization of CRBN Pro352, mutated to Ser in patients. (E) Localization of CRBN Cys366, mutated to Tyr in patients. (F) Localization of CRBN Phe381, mutated to Ser in patients.

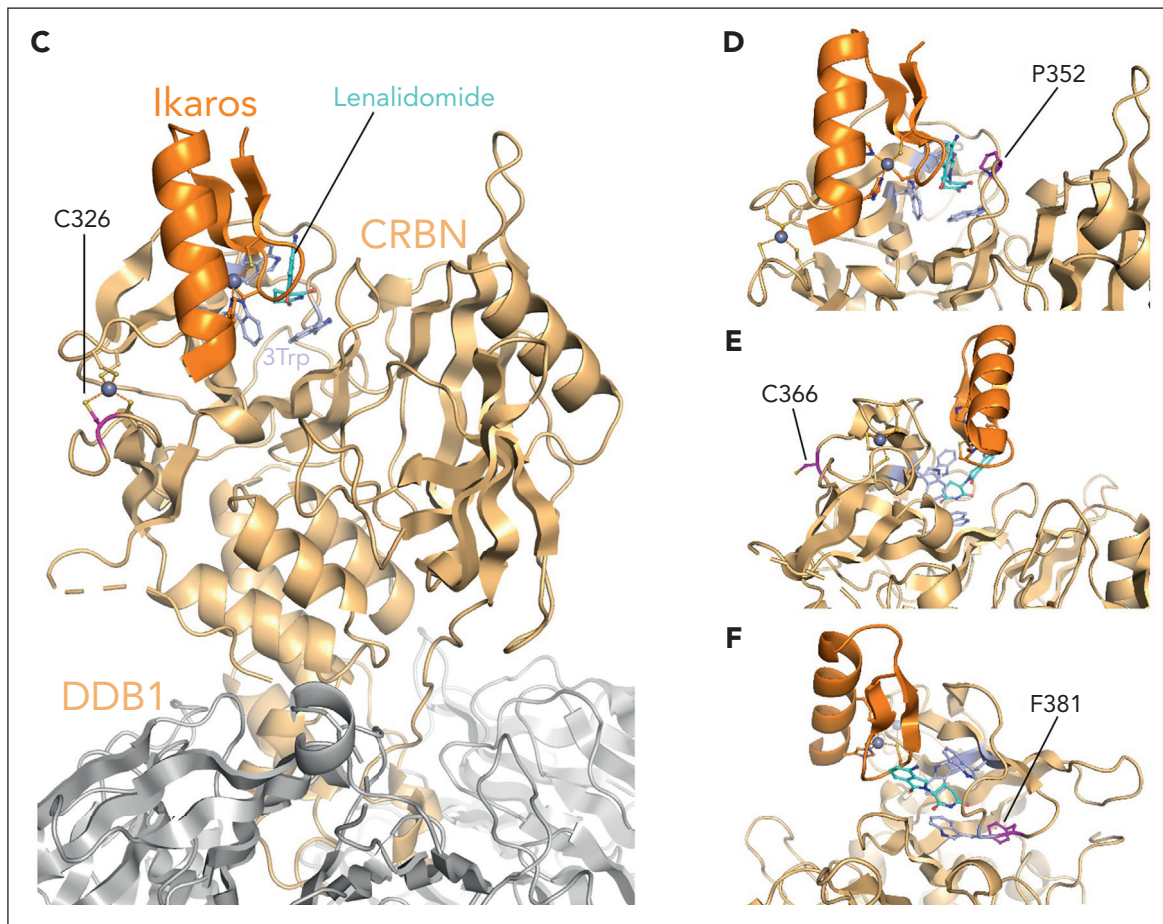


Figure 4 (continued)

and hence, its mutation could be expected to strongly affect CRBN function (Figure 4D). However, Mezi led to partial degradation of Aiolos (Figure 3A-B; supplemental Figures 7A-B and 9), Ikaros, and ZFP91 (Figure 4A; supplemental Figures 8A and 9) and downregulation of IRF4 (more prominently demonstrated in MM1.s^{CRBNKO} clone 2, supplemental Figure 7A-C) and MYC (Figure 4A), with a slight reduction in cell viability not observed with any of the other compounds (Figure 2A; supplemental Figure 4A).

In contrast mutation p.C366Y (Figure 4E) would be expected to have no or only marginal effect on CRBN function based on the structural analysis. This residue is surface exposed and is far away from the IMiDs and neosubstrate-binding sites (Figure 4E). A partial response to CELMoDs, and none to IMiDs, was seen with this mutant (Figures 2A and 4B; supplemental Figures 4A, 7A, and 9; mutations highlighted in orange). It could be hypothesized that the presence of a hydrophobic bulkier amino acid tyrosine instead of cysteine might compromise the folding and/or dynamics of the protein, but further investigations would be needed to clarify, which is beyond the scope of this study.

Determining the effect of CRBN mutations in a heterozygous model

In the experiments described above, all CRBN mutations were investigated in an effective homozygous, clonal state (CRBN KO

with re-expression of each mutant). This provides both critical biochemical information and important clinical information given that if the mutation was sufficient to induce complete resistance to subsequent generations of IMiDs/CELMoDs administered to patients, then an outgrowth of the resistant clone would be expected rapidly. However, these mutations are often encountered in a heterozygous and/or subclonal state in patients (supplemental Table 2), so additional experiments were conducted to explore their likely impact in these circumstances. Therefore, CRBN mutations p.W386A and p.H397Y (leading to loss of CRBN function), p.D50H and p.R283K (no apparent effect on CRBN function), p.C326G and p.F381S (agent-dependent effect on CRBN function), and the WT plasmid were introduced in the parental MM1.s cell line, to mimic a heterozygous state (supplemental Figure 10). Interestingly, introduction of WT CRBN (MM1.s^{WT/WT}) led to significantly higher CRBN levels and increased response to IMiDs and CELMoDs compared with parental MM1.s (supplemental Figure 10B; Figure 5). The response to Pom and Mezi did not differ between MM1.s^{WT/WT} and MM1.s^{WT/D50H} or MM1.s^{WT/R283K} (Figure 5; supplemental Figure 11). This confirms the absence of functional impact of these mutations as seen in the homozygous models and also suggests there was no dominant negative impact of the mutations on WT CRBN function. For the heterozygous models of p.C326G, p.F381S, p.W386A, and p.H397Y, the impact of each mutation is evident with decreased

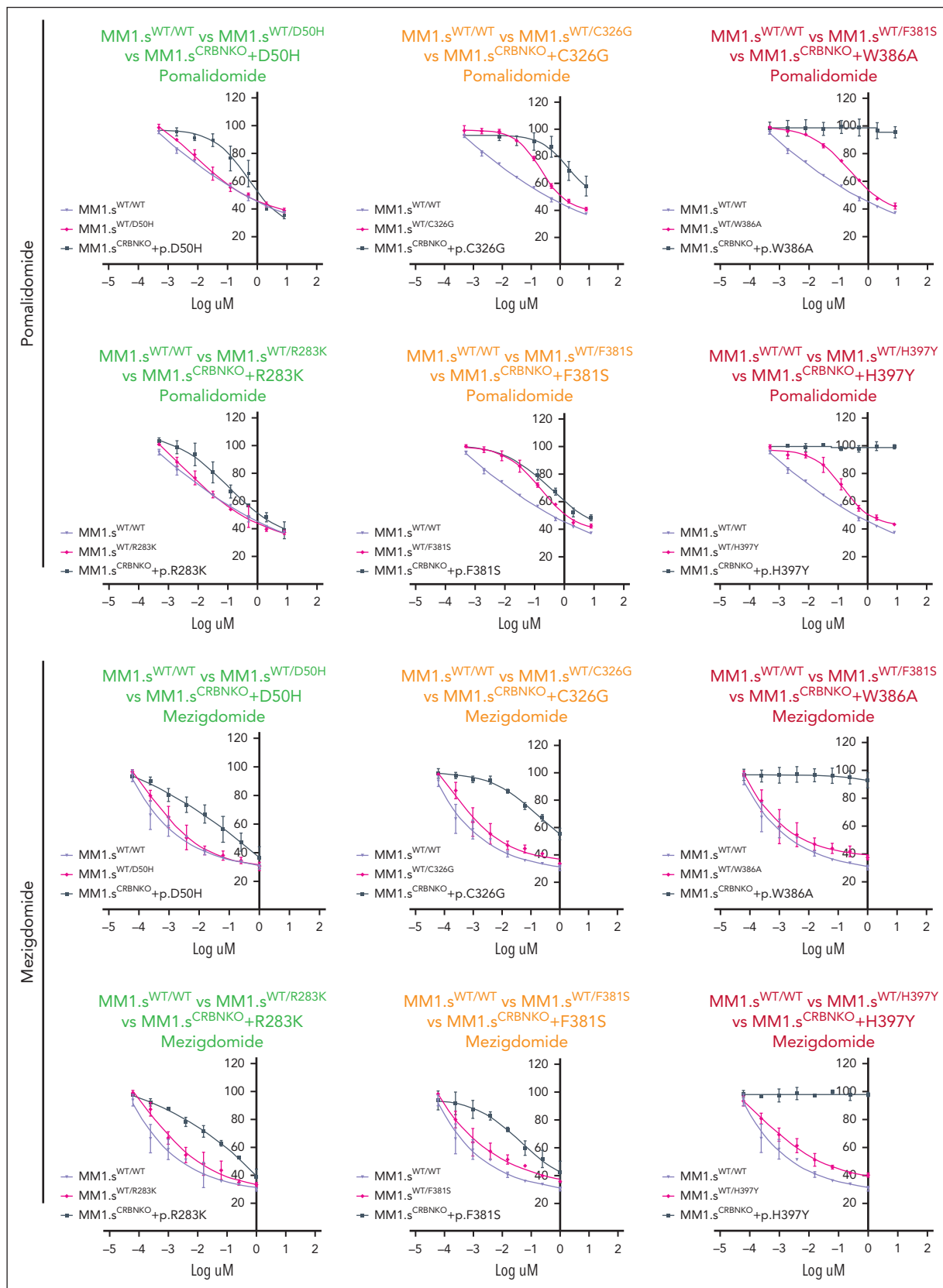


Figure 5. The effect of CRBN mutations in a heterozygous model. (A) GI50 cell viability measurements for the CRBN^{WT/WT} cell line (WT plasmid overexpression) and each cell line with heterozygous CRBN (mutated CRBN overexpression). The corresponding CRBN^{KO} clone 1 homozygous mutation GI50 curve from Figure 2A has been added to each graph (gray) only to aid in the visual comparison between heterozygous and homozygous mutations. The color of the title for each graph denotes the effect on cell viability associated with each mutation in its homozygous state, where green is associated with reduction in cell viability comparable with parental MM1.s, red denotes no reduction in cell viability, and orange highlights the mutations whose presence leads to partial reduction in cell viability. Cells were treated with DMSO or increasing

response to Pom particularly with lower drug concentrations, both for mutations with an agent-dependent effect (p.C326G and p.F381S) and those shown to completely abolish CRBN function (p.W386A and p.H397Y) in the homozygous models. However, Mezi seemed to overcome the impact of all 4 of these mutations, likely explained by the increased potency of Mezi using the functional CRBN present in the heterozygous model cell lines.

MD modeling to explore the effect of mutations close to the IMiDs' binding site

Two of the mutations with an agent-dependent effect on CRBN function p.P352S and p.F381S (selected as they were located closest to the binding site) underwent MD simulations aiming to further explore the structural features responsible for the differential response seen. A crystallographic structure of the DDB1/CRBN/Len complex was solved at 2.00 Å resolution in-house and used as a reference for modeling the WT and 2 selected mutant constructs. Publicly available structural data available for CRBN in complex with Iber and Mezi are at relatively low resolution (>3 Å) with only weak electron density for the molecular glues and some of their surrounding residues. This insufficient confidence on the exact positioning of the corresponding atoms in the PDB models, which would be required to ensure reliable simulations, precluded a side-by-side comparison between IMiDs and CELMoDs.

MD trajectories were analyzed by calculating the RMSD of atomic positions of Len and CRBN-binding site residues, which confirmed their relative stability along the simulations (supplemental Figure 12A-B). No clear difference was found in the position of Len heavy atoms throughout the MDs of the mutant constructs compared with the WT. However, slightly larger RMSD values were obtained for CRBN-binding site residues in the MD simulations of the F381S construct over the WT, despite them being very close on average (median values of 1.31 Å and 1.19 Å across all simulation replicas, respectively).

The steep structure-activity relationship typically observed in molecular glues-induced targeted protein degradation prompted more detailed analysis of the conformations sampled during the simulations. A structural overlay between the reference crystal structure and the most representative conformations obtained by clustering the MD trajectories of the 2 mutant constructs showed that most residues in the CRBN pocket conserved highly similar side chain orientations, although subtle differences could be observed particularly for residues more exposed to the bulk solvent (supplemental Figure 12C). Some of these (eg, H353, H357, H397) are interface residues known to play a role in the recruitment of neosubstrate degrons, and thus, only specific side chain conformations may be tolerated. Furthermore, the phthalimidine ring system of Len in the representative conformation bound to the P352S mutant construct was found to sit out of the plane occupied in the crystal structure with the WT, likely due to the steric hindrance caused by the mutant serine residue. It was hypothesized that this could interfere with the recruitment of neosubstrates, as

suggested by the increased number of unfavorable contacts predicted in the representative conformation of the mutant construct between Len and IKZF1 degron atoms in PDB 6h0f after alignment on the backbone atoms of CRBN-binding site residues (Figure 6A-B). To probe this throughout the MD simulations, clash volumes were calculated across all trajectory frames between the heavy atoms of Len and the aligned IKZF1 degron (Figure 6C). Clashes were found to be substantially larger in the simulations of the P352S mutant construct than the WT (median values of 37 Å³ and 0.3 Å³, respectively), which further suggests that the conformational change predicted in the binding mode of Len upon proline to serine mutation could alter the shape complementarity with the degron and thus explain the observed lack of neosubstrate degradation by Len.

Clash volume values calculated in the simulations of the F381S construct were distributed mostly in between those found with the WT and P352S constructs (Figure 6C, median of 7.3 Å³), in line with the intermediate degradation potency and cell viability experimentally observed with Len against this mutant. Comparing the representative conformation obtained from clustering with the reference crystal structure showed large deviations for some residues found close to the F381S mutation (Figure 7A) but only small deviations when considering CRBN residues proximal to Len (Figure 7B). This suggests that local conformational changes induced by the F381S mutation can be accommodated closer to the degron region, as also shown by the difference in RMSD values calculated for the binding site and the mutation site (Figure 7C). However, the strong perturbations in the positioning of residues close to the mutation site, which is located at the core of the TBD domain, could have an overall detrimental effect on the stability and folding of the domain and in turn on the ability to interact with neosubstrates. It could be hypothesized that the partial rescue of CRBN activity observed with CELMoDs in the p.F381S cell line could be ascribed to their enhanced ability to stabilize CRBN compared with IMiDs.^{2,11}

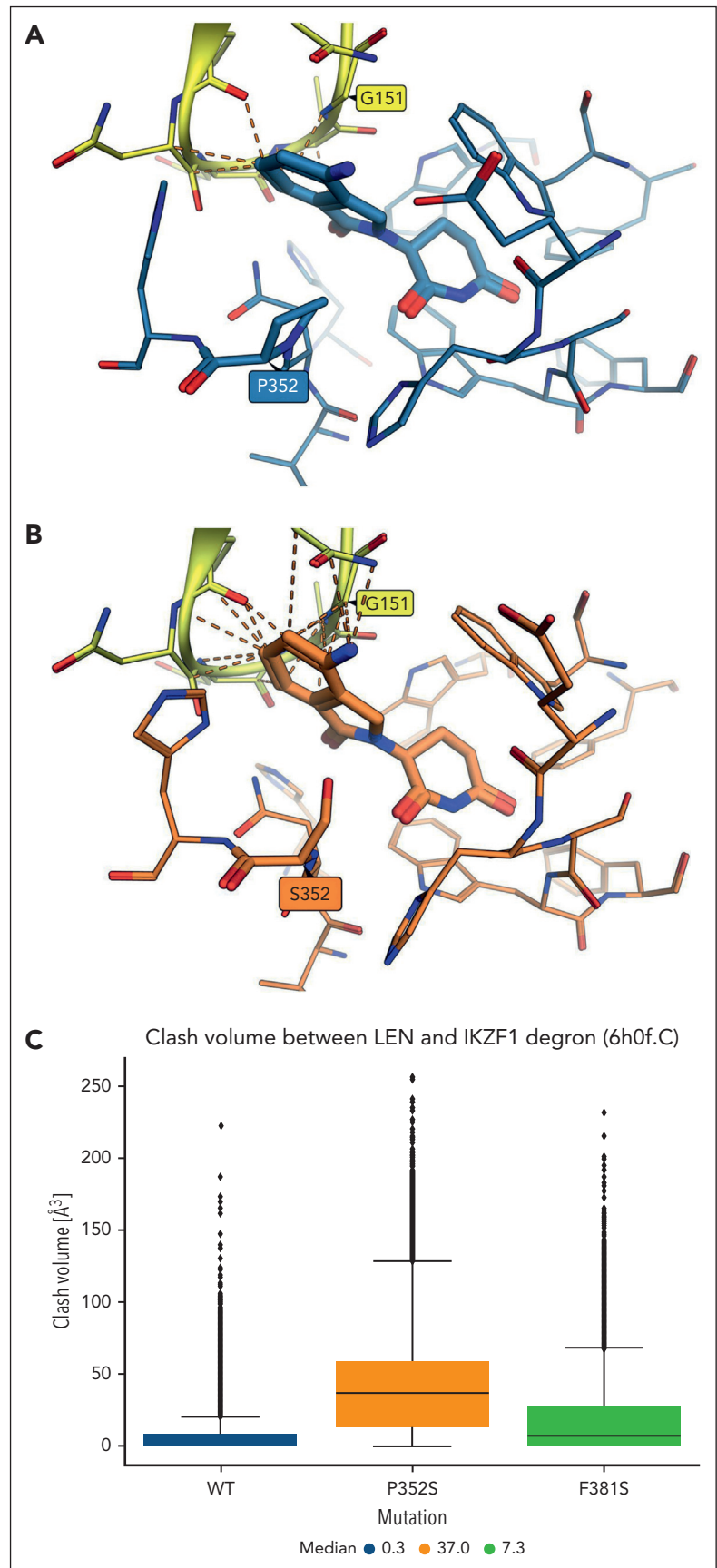
Discussion

As sequencing panels become more widely available as part of myeloma patient diagnostics, it is of increasing importance to understand the functional impact of mutations identified.²⁴ Data presented here highlight key differences in the functional impact of different CRBN missense mutations. This is despite them all having been identified in patient data sets, for patients relapsing on IMiD therapy, so it could have been assumed that they might all be of clinical relevance. These findings underline the importance of such functional analyses, especially if clinical treatment decisions may result from the genetic reporting.

Functional validation demonstrated that all mutations in the Lon protease-like domain and DDB1-binding helix-bundle sub-domain had no impact of CRBN function in our homozygous model, with similar responses to both IMiDs and CELMoDs as WT CRBN re-expression. Indeed, tolerated mutations (with preserved CRBN function) were even identified in the TBD such

Figure 5 (continued) concentrations of Pom (maximum concentration 8 μM) and Mezi (maximum concentration 1 μM) for 5 days. Cell viability was determined using the CellTiter-Blue assay and expressed as a % of DMSO control. Results are the mean ± SEM of n = 3 biological replicates.

Figure 6. Clashes predicted between the IKZF1 degron and Len bound to WT and p.P352S CRBN constructs. (A) Unfavorable contacts shown as orange dashes between Len bound to WT CRBN (C atoms shown in light blue with proline 352 highlighted) and IKZF1 degron atoms from PDB 6h0f (C atoms in yellow with glycine 151 highlighted) after structural alignment on CRBN-binding site residues. (B) A larger number of clashes is predicted between the IKZF1 degron and Len bound to the p.P352S CRBN construct (representative conformation from MD; C atoms in orange with serine 352 highlighted). (C) Distribution of clash volumes calculated between heavy atoms of the IKZF1 degron and Len in MD trajectory frames of the WT (blue box), p.P352S (orange), and p.F381S (green) CRBN constructs.



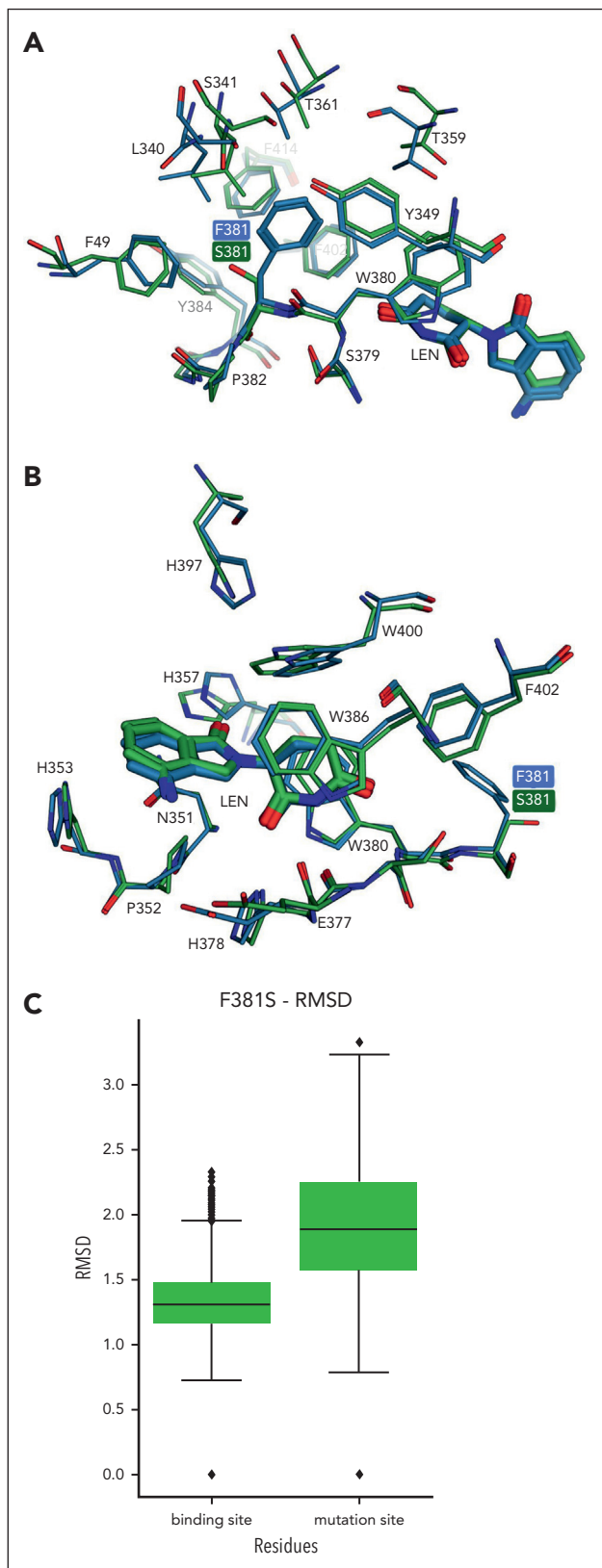


Figure 7. Analysis of conformational changes predicted by MD simulations of the p.F381S CRBN construct. (A) Conformations of residues located in the surroundings of the p.F381S mutation are shown in the representative conformation from MD simulations of the mutant construct (C atoms in green) compared with the crystal structure of WT CRBN (C atoms in light blue). (B) A similar comparison focused on Len binding site shows smaller deviations mainly for residues exposed

as p.A347V and p.W415G, meaning that using a too simplistic approach to localizing mutations of clinical relevance should be avoided. This was corroborated in our heterozygous model, also demonstrating that such mutations do not seem to have a dominant negative effect. For patients whose myeloma cells harbor these mutations, there is no evidence to suggest that they would have an impaired, myeloma cell-intrinsic, response to repeat IMiD exposure. This raises the question as to why these mutations were identified in patients (in the data sets from which the mutations modeled were selected). It might be that they were passengers rather than drivers, with other events either myeloma cell intrinsic or extrinsic playing a role in the development of resistance.¹ It should be noted that this report presents the impact of mutations at equal or greater CRBN expression to WT cell lines, and it might not reflect the outcome observed in a patient presenting with low CRBN levels.

More in line with what could have been expected in all patients relapsing after IMiD therapy, one mutation, p.H397Y, completely abrogated CRBN function with all IMiDs and CELMoDs tested. Unfortunately, these data suggest that even the more potent CELMoD agents would be of little benefit to patients harboring such a deleterious mutation at high clonal fraction.

Of key interest were those mutations identified where results demonstrated a differential response between IMiDs and CELMoDs in our homozygous model. The common element between these 4 mutations is that the more potent CELMoD compounds, and Mezi in particular, led to degradation of key neosubstrates and elicited a viability response, whereas IMiDs gave rise to no or little effect. CELMoDs have been shown to be able to stabilize CRBN in its closed conformation¹¹ more efficiently than IMiDs, which is the conformation leading to the recruitment of CRBN neosubstrates. In the context of these mutations, this difference could potentially lead to partial rescue of function of otherwise severely destabilized and/or functionally impaired CRBN mutant protein. Even if they could drive conformation rearrangement in only a small proportion of CRBN protein molecules, this may be sufficient to induce a degradation response and myeloma cell death. Importantly, these observations indicate that using CELMoDs in patients whose myeloma harbors these mutations may be a viable option even after the development of IMiD resistance.

This concept is supported by the work of Hanzl et al³⁵ who studied the impact of CRBN mutations in a colon carcinoma background on response to G1 to S phase transition protein 1 (GSPT-1) degrading molecular glues and proteolysis-targeting chimeras (PROTACs) as opposed to the IMiDs/CELMoDs in our study. Similar to our findings, they determined the CRBN sensor loop and 3-Trp pocket sequences as hot spots for mutations likely to be disruptive to agent activity, highlighting the amino acid H397 in particular, whereas some sites presented with a differential response depending on the chemical agent used.

The mutations selected for this study occurred at various variant allele frequencies in the original reports, and most were

Figure 7 (continued) to the solvent (eg, H357, H397, W400). (C) Distribution of RMSD values calculated on MD simulations of the p.F381S construct for residues located in both binding site and mutation site (5 Å from Len and the mutated residue, respectively).

subclonal. Nevertheless, understanding the impact of mutations in the homozygous model, on a structural level, is important given that if the mutation was sufficient to induce complete resistance to subsequent generations of IMiDs/CELMoDs administered to patients, then an outgrowth of the resistant clone would be expected rapidly, leading to only very short-term responses. However, to explore the heterozygous state further, an additional model was generated expressing selected mutations in parental MM1.s cells to generate a cell model in which WT and mutant CRBN would both be present. This work highlighted that the most potent CELMoD, Mezi, could overcome expression of the mutations in cell lines with sufficient residual WT CRBN. However, there were some limitations to our overexpression system, which generated cell lines with likely the same amount of functional CRBN as parental cells with additional mutant CRBN also expressed. A model using CRISPR editing technology to generate both heterozygous and homozygous mutants may more faithfully recapitulate the disease state in patients and could be explored in future studies.

Assessing in vitro the effect of all mutations identified in myeloma patients across the gene is clearly not feasible, particularly for genes in which mutations are not restricted to hot spot sites, and indeed this project focused on selected mutations from across the sequence of CRBN. Structural biology analysis may be more feasible for predicting mutational impact, and we sought to explore this alongside the functional studies. Indeed, the analysis of static 3-D models was able to predict the functional outcome of most mutations selected for this study. MD modeling provided further information for the IMiD Len, which matched our in vitro results. However, using these methodologies to dissect the precise activity of lber and Mezi is currently challenged by the lack of sufficiently high-resolution structural data with these compounds bound to CRBN to perform this type of analysis. Additional work to demonstrate differences in physical interactions using a system such as Turbo-ID for proximity biotinylation would also add further to our understanding of these interactions in the future but were beyond the scope of the current study. Taken together these findings suggest that the overall clinical impact of CRBN missense mutations might be lower than previously thought, given that not all mutations identified seem to have a functional impact and some with an impact on IMiD response may be overcome with CELMoD use. It is difficult to precisely quantify the frequency of each type of mutation in relapsed myeloma after each therapy given that previous reports have been heterogeneous and not all identified mutations have been modeled. On balance a trial of CELMoDs in patients with CRBN mutations after relapsing on IMiDs would likely be warranted because it is difficult to conclude definitively that a patient will not respond either on the basis of having a mutation that can be structurally overcome or due to having sufficient residual WT CRBN to bind the more potent compounds.

Overall, the results presented here may have important implications for the interpretation of CRBN sequencing

results from patients relapsing on IMiDs for future therapy decisions.

Acknowledgments

The authors acknowledge and are grateful for the contribution of Craig McAndrew and Rob Van Montfort from The Hit Discovery and Structural Design team at the Centre for Cancer Drug Discovery, The Institute of Cancer Research for production of recombinant CRBN/DDBI protein and structure determination. The authors thank the staff of DIAMOND Light Source for their support during crystallographic data collection. The authors acknowledge the support of The Centre for Protein Degradation at The Institute of Cancer Research.

This work was primarily funded by a Cancer Research UK (CRUK) Clinician Scientist Fellowship grant C47608/A29957 (C.P.) and supported by additional funding from Cancer Research Innovation in Science (CRIS) Cancer Foundation and The Institute of Cancer Research.

Authorship

Contribution: Y.C., A.S., Y.-V.L.B., and C.P. conceived the project, designed the analysis, and drafted the manuscript; Y.C., S. Morales, and S. Martin conducted wet-lab experiments; A.S. and Y.-V.L.B. conducted computational modeling; B.W. performed sequencing analysis; J.C. synthesized compounds; and all authors analyzed and interpreted the data for the analysis, and contributed to critically revising the manuscript and approved the final submitted version.

Conflict-of-interest disclosure: The Institute of Cancer Research has a commercial interest in the development of compounds targeting CRL4-CRBN E3-ubiquitin ligases. C.P. has received honoraria from Celgene/Bristol Myers Squibb for advisory boards, educational talks, and participation in data monitoring boards. The remaining authors declare no competing financial interests.

ORCID profiles: Y.C., [0009-0002-2831-1321](https://orcid.org/0009-0002-2831-1321); A.S., [0000-0003-3287-6210](https://orcid.org/0000-0003-3287-6210); S.B., [0000-0001-8080-0937](https://orcid.org/0000-0001-8080-0937); Y.L., [0000-0002-0420-214X](https://orcid.org/0000-0002-0420-214X); B.W., [0000-0002-8615-6254](https://orcid.org/0000-0002-8615-6254); J.C., [0000-0001-9141-5452](https://orcid.org/0000-0001-9141-5452); Y.-V.L.B., [0000-0002-6850-9706](https://orcid.org/0000-0002-6850-9706); C.P., [0000-0002-7190-0028](https://orcid.org/0000-0002-7190-0028).

Correspondence: Charlotte Pawlyn, The Institute of Cancer Research, 15 Cotswold Rd, Sutton, London SM2 5NG, United Kingdom; email: charlotte.pawlyn@icr.ac.uk.

Footnotes

Submitted 2 July 2024; accepted 19 December 2024; prepublished online on *Blood* First Edition 22 January 2025. <https://doi.org/10.1182/blood.2024025861>.

The crystallographic structure of the DNA damage-binding protein 1/ cereblon/lenalidomide complex has been deposited in the Protein Data Bank (accession code 9FXJ).

The online version of this article contains a data supplement.

There is a [Blood Commentary](#) on this article in this issue.

The publication costs of this article were defrayed in part by page charge payment. Therefore, and solely to indicate this fact, this article is hereby marked "advertisement" in accordance with 18 USC section 1734.

REFERENCES

- Bird S, Pawlyn C. IMiD resistance in multiple myeloma: current understanding of the underpinning biology and clinical impact. *Blood*. 2023;142(2):131-140.
- Matyskiela ME, Zhang W, Man HW, et al. A cereblon modulator (CC-220) with improved degradation of Ikaros and Aiolos. *J Med Chem*. 2018;61(2):535-542.
- Bjorklund CC, Kang J, Amatangelo M, et al. lberdomide (CC-220) is a potent cereblon E3 ligase modulator with antitumor and immunostimulatory activities in lenalidomide- and pomalidomide-resistant multiple

- myeloma cells with dysregulated CRBN. *Leukemia*. 2020;34(4):1197-1201.
4. Hansen JD, Correa M, Nagy MA, et al. Discovery of CRBN E3 ligase modulator CC-92480 for the treatment of relapsed and refractory multiple myeloma. *J Med Chem*. 2020;63(13):6648-6676.
 5. Richardson PG, Trudel S, Popat R, et al. Mezigdomide plus dexamethasone in relapsed and refractory multiple myeloma. *N Engl J Med*. 2023;389(11):1009-1022.
 6. Thakurta A, Gandhi AK, Waldman MF, et al. Absence of mutations in cereblon (CRBN) and DNA damage-binding protein 1 (DDB1) genes and significance for IMiD therapy. *Leukemia*. 2014;28(5):1129-1131.
 7. Ito T, Ando H, Suzuki T, et al. Identification of a primary target of thalidomide teratogenicity. *Science*. 2010;327(5971):1345-1350.
 8. Krönke J, Hurst SN, Ebert BL. Lenalidomide induces degradation of IKZF1 and IKZF3. *Onc Immunology*. 2014;3(7):e941742.
 9. Holstein SA, McCarthy PL. Immunomodulatory drugs in multiple myeloma: mechanisms of action and clinical experience. *Drugs*. 2017;77(5):505-520.
 10. Petzold G, Fischer ES, Thomä NH. Structural basis of lenalidomide-induced CK1 α degradation by the CRL4 CRBN ubiquitin ligase. *Nature*. 2016;532(7597):127-130.
 11. Watson ER, Novick S, Matsykiela ME, et al. Molecular glue CELMoD compounds are regulators of cereblon conformation. *Science*. 2022;378(6619):549-553.
 12. Sievers QL, Petzold G, Bunker RD, et al. Defining the human C2H2 zinc finger degrome targeted by thalidomide analogs through CRBN. *Science*. 2018;362(6414):eaat0572.
 13. Fischer ES, Böhm K, Lydeard JR, et al. Structure of the DDB1-CRBN E3 ubiquitin ligase in complex with thalidomide. *Nature*. 2014;512(7512):49-53.
 14. Chamberlain PP, Lopez-Girona A, Miller K, et al. Structure of the human cereblon-DDB1-lenalidomide complex reveals basis for responsiveness to thalidomide analogs. *Nat Struct Mol Biol*. 2014;21(9):803-809.
 15. Lupas AN, Zhu H, Korycinski M. The thalidomide-binding domain of cereblon defines the CULT domain family and is a new member of the β -tent fold. *PLoS Comput Biol*. 2015;11(1):e1004023.
 16. Ichikawa S, Flaxman HA, Xu W, et al. The E3 ligase adapter cereblon targets the C-terminal cyclic imide degron. *Nature*. 2022;10(7933):775-782.
 17. Matsykiela ME, Lu G, Ito T, et al. A novel cereblon modulator recruits GSPT1 to the CRL4 CRBN ubiquitin ligase. *Nature*. 2016;535(7611):252-257.
 18. Matsykiela ME, Clayton T, Zheng X, et al. Crystal structure of the SALL4-pomalidomide-cereblon-DDB1 complex. *Nat Struct Mol Biol*. 2020;27(4):319-322.
 19. Wang ES, Verano AL, Nowak RP, et al. Acute pharmacological degradation of Helios destabilizes regulatory T cells. *Nat Chem Biol*. 2021;17(6):711-717.
 20. Shaffer AL, Emre NCT, Lamy L, et al. IRF4 addiction in multiple myeloma. *Nature*. 2008;454(7201):226-231.
 21. Liu J, Hideshima T, Xing L, et al. ERK signaling mediates resistance to immunomodulatory drugs in the bone marrow microenvironment. *Sci Adv*. 2021;7(23):eabg2697.
 22. Dimopoulos MA, Palumbo A, Corradini P, et al. Safety and efficacy of pomalidomide plus low-dose dexamethasone in STRATUS (MM-010): a phase 3b study in refractory multiple myeloma. *Blood*. 2016;128(4):497-503.
 23. Gooding S, Ansari-Pour N, Towfic F, et al. Multiple cereblon genetic changes are associated with acquired resistance to lenalidomide or pomalidomide in multiple myeloma. *Blood*. 2021;137(2):232-237.
 24. Sudha P, Ahsan A, Ashby C, et al. Myeloma genome project panel is a comprehensive targeted genomics panel for molecular profiling of patients with multiple myeloma. *Clin Cancer Res*. 2022;28(13):2854-2864.
 25. The PyMOL Molecular Graphics System. Version 2.5.5. Schrödinger, LLC; 2023. Accessed 5 June 2024. <https://pymol.org>
 26. Kortüm KM, Mai EK, Hanafiah NH, et al. Targeted sequencing of refractory myeloma reveals a high incidence of mutations in CRBN and Ras pathway genes. *Blood*. 2016;128(9):1226-1233.
 27. Barrio S, Munawar U, Zhu YX, et al. IKZF1/3 and CRL4^{CRBN} E3 ubiquitin ligase mutations and resistance to immunomodulatory drugs in multiple myeloma. *Haematologica*. 2020;105(5):E237-E241.
 28. Jones JR, Barber A, Le Bihan YV, et al. Mutations in CRBN and other cereblon pathway genes are infrequently associated with acquired resistance to immunomodulatory drugs. *Leukemia*. 2021;35(10):3017-3020.
 29. Egan JB, Kortuem KM, Kurdoglu A, et al. Extramedullary myeloma whole genome sequencing reveals novel mutations in Cereblon, proteasome subunit G2 and the glucocorticoid receptor in multi drug resistant disease. *Br J Haematol*. 2013;161(5):748-751.
 30. Sastry GM, Adzhigirey M, Day T, Annabhimoju R, Sherman W. Protein and ligand preparation: parameters, protocols, and influence on virtual screening enrichments. *J Comput Aided Mol Des*. 2013;27(3):221-234.
 31. Schrödinger Suite v2023-3. Schrödinger, LLC; 2023. Accessed 5 June 2024. <https://www.schrodinger.com/>
 32. Bowers KJ, Chow E, Xu H, et al. Scalable algorithms for molecular dynamics simulations on commodity clusters. Proceedings of the ACM/IEEE Conference on Supercomputing (SC06); 11-17 November 2006; Tampa, FL. Accessed 5 June 2024. <https://dl.acm.org/doi/proceedings/10.1145/1188455>
 33. Molecular Operating Environment. Chemical Computing Group; 2024. Accessed 5 June 2024. <https://www.chemcomp.com/>
 34. Ito T, Handa H. Cereblon and its downstream substrates as molecular targets of immunomodulatory drugs. *Int J Hematol*. 2016;104(3):293-299.
 35. Hanzl A, Casement R, Imrichova H, et al. Functional E3 ligase hotspots and resistance mechanisms to small-molecule degraders. *Nat Chem Biol*. 2023;19(3):323-333.

© 2025 American Society of Hematology. Published by Elsevier Inc. Licensed under Creative Commons Attribution-NonCommercial-NoDerivatives 4.0 International (CC BY-NC-ND 4.0), permitting only noncommercial, nonderivative use with attribution. All other rights reserved.